



Cite this: *J. Mater. Chem. C*, 2022, 10, 7443

Received 1st March 2022,
Accepted 18th April 2022

DOI: 10.1039/d2tc00850e

rsc.li/materials-c

High-performance ultra-narrow-band green-emitting phosphor $\text{LaMgAl}_{11}\text{O}_{19}:\text{Mn}^{2+}$ for wide color-gamut WLED backlight displays†

Zhangyue Wu,^a Chao Li,^{id} *^a Feng Zhang,^{id} *^a Shixiang Huang,^a Feijiu Wang,^{id} *^a
Xiaoming Wang,^{id} ^b and Huan Jiao,^{id} *^b

Explorations of narrow-band green-emitting phosphors have attracted much attention due to their great application potential in wide color-gamut WLED backlight displays. Herein, a high-performance narrow-band green-emitting phosphor $\text{LaMg}_{0.72}\text{Al}_{11}\text{O}_{19}:\text{0.28Mn}^{2+}$ (LMAO:0.28Mn²⁺) was synthesized with a high activator doping content. The LMAO:0.28Mn²⁺ green phosphor exhibits an ultra-narrow-band green emission peaking at 517 nm with an intriguing full width at half maximum of ~24 nm. The LMAO:0.28Mn²⁺ not only has a good internal quantum efficiency of 97.6% but also has an excellent low thermal quenching performance (92.3% peak intensity @423 K), especially an excellent resistance to color drifting (3.82‰ @423 K). A WLED device fabricated using LMAO:0.28Mn²⁺, $\text{K}_2\text{SiF}_6:\text{Mn}^{4+}$ phosphors and a blue chip shows a wide color-gamut of 131% National Television System Committee (NTSC) standard, making LMAO:0.28Mn²⁺ a highly promising candidate for wide color-gamut WLED backlights. The new strategy can be easily expanded to other systems and boost the development of efficient narrow-band emitting phosphors.

1. Introduction

In recent decades, phosphor-converted white LEDs (pc-WLEDs) have been mainstream candidates for liquid crystal display (LCD) backlights due to their outstanding properties such as low power consumption, high brightness, low heat emission, environment-friendliness and long lifetime.^{1–3} Compared with other display technologies, narrow-band phosphors have been

recognized as key enablers for color gamut backlights in LCDs.^{4–6} Many high-efficiency narrow-band green emitters have been developed to realize wide color-gamut backlight displays. CdSe/ZnS and perovskite quantum dots (QDs) CsPbBr_3 are promising candidates due to the super-narrow FWHM of ~20 nm, but Cd and Pb are toxic, and CsPbBr_3 has limited moisture resistance and poor thermal stability, which inevitably restricts their practical application.⁷ Furthermore, many lanthanide activated (e.g., Eu^{2+} , Tb^{3+}) efficient narrow-band green emitting phosphors have been developed, such as $\beta\text{-SiAlON}:\text{Eu}^{2+}$ (FWHM ~55 nm), $\gamma\text{-AlON}:\text{Mn}^{2+}$, Mg^{2+} (FWHM ~44 nm), $\text{Ba}[\text{Li}_2(\text{Al}_2\text{Si}_2)\text{N}_6]:\text{Eu}^{2+}$ (FWHM ~57 nm), $\text{Ba}_2\text{LiSi}_7\text{AlN}_{12}:\text{Eu}^{2+}$ (FWHM ~61 nm), $\text{SrGa}_2\text{S}_4:\text{Eu}^{2+}$ (FWHM ~47 nm), $\text{RbLi}(\text{Li}_3\text{SiO}_4)_2:\text{Eu}^{2+}$ (FWHM ~42 nm) and $\text{RbNa}(\text{Li}_3\text{SiO}_4)_2:\text{Eu}^{2+}$ (FWHM ~41 nm).^{4,8–13} However, these materials all suffer from the problems of high cost, harsh synthesis conditions and poor stability. To achieve cheaper and more stable narrow green-emitting phosphors, some transition-metal-activated (e.g., Mn^{2+}) silicate and aluminosilicate phosphors have been investigated, such as $\text{Zn}_2\text{SiO}_4:\text{Mn}^{2+}$ (FWHM ~42 nm), $\text{MgAl}_2\text{O}_4:\text{Mn}^{2+}$ (FWHM ~35 nm), $\text{BaZnAl}_{10}\text{O}_{17}:\text{Mn}^{2+}$ (FWHM ~31 nm), $\text{BaAl}_{12}\text{O}_{19}:\text{Mn}^{2+}$ (FWHM ~26 nm) and $\text{Sr}_2\text{MgAl}_{22}\text{O}_{36}:\text{Mn}^{2+}$ (FWHM ~26 nm).^{7,14–17} It is a great possibility to achieve a wide color-gamut (>120% NTSC) WLED device by using a suitable Mn^{2+} based phosphor as the green emitter. However, the absorption and emission of Mn^{2+} belong to the spin-forbidden d-d transition and depend strongly on the host lattice.^{18,19} It is a fundamental challenge to obtain a cheaper and highly efficient Mn^{2+} based narrow-band green emitting phosphor.

Due to the energy transfer interaction between luminescence centers and luminescence killer centers,^{8,20–22} there is optimal doping content for an activator in a phosphor. When the activator content exceeds its optimal value, the concentration-quenching effect can occur and the emission intensity can decrease.^{23,24} While the energy transfer can be reduced between long-distance luminescence centers and the

^a Key Lab of Photovoltaic Materials of Henan Province, Henan University, Kaifeng, 475001, P. R. China. E-mail: lichao_henan@163.com, zhangfeng.home@163.com

^b Key Laboratory of Macromolecular Science of Shaanxi Province, Shaanxi Engineering Laboratory for Advanced Energy Technology, Shaanxi Key Laboratory for Advanced Energy Devices, School of Chemistry & Chemical Engineering, Shaanxi Normal University, Xi'an 710062, P. R. China. E-mail: jiaohuan@snnu.edu.cn

† Electronic supplementary information (ESI) available. See DOI: <https://doi.org/10.1039/d2tc00850e>

phosphor can achieve efficient emission in spite of high activator content.²⁵ If there is only one site for the activator to occupy, it will contribute to the narrow band emission for the phosphor.²⁶ Thus, designing activator doping at independently remote isolated sites can not only be beneficial to the narrow band emission but also enlarge the optimal doping content of the activator to realize high content activators inducing highly efficient emission for phosphors. $\text{LaMgAl}_{11}\text{O}_{19}$ (LMAO) crystallizes in a slightly distorted magnetoplumbite $\text{PbFe}_{12}\text{O}_{19}$ (M-type) structure with hexagonal space group $P6_3/mmc$.²⁷ There is only one Mg^{2+} site. In particular, the distances between isolated Mg^{2+} sites are remote. In this work, a high-performance narrow-band green-emitting phosphor $\text{LaMg}_{0.72}\text{Al}_{11}\text{O}_{19}:0.28\text{Mn}^{2+}$ (LMAO:0.28 Mn^{2+}) was synthesized with a high Mn^{2+} doping content. LMAO:0.28 Mn^{2+} exhibits an impressive ultra-narrow-band emission peaking at 517 nm with a fwhm of ~ 24 nm and a high internal quantum efficiency (IQE) up to 97.6%. Furthermore, LMAO:0.28 Mn^{2+} shows an outstanding thermal quenching resistance, maintaining 92.3% peak intensity and 110.1% integrated intensity at 423 K, which is superior to commercial narrow-band green-emitting phosphor $\beta\text{-SiAlON}:\text{Eu}^{2+}$. A pc-wLED device fabricated by LMAO:0.28 Mn^{2+} , $\text{K}_2\text{SiF}_6:\text{Mn}^{4+}$ (KSF: Mn^{4+}) phosphors and a blue InGaN chip exhibits a wide color gamut up to 131% NTSC and 97.8% Rec. 2020. This work opens a new path to develop high-performance narrow-band green emitting phosphors for wide color-gamut wLED backlight displays.

2. Results and discussion

The crystal structure of LMAO is shown in Fig. 1a. There is one La and one Mg crystallographic site and five distinct Al crystallographic sites. Mg1 and Al3 are co-occupied with a ratio of 1 : 1 and exhibit 4-fold coordination with neighboring O atoms. The independent Mg site exhibits a highly symmetric tetrahedron coordination environment, which is in favor of small Stokes

shift and narrow-band green emission.²⁶ The structure framework of LMAO is composed of $[\text{Mg1}/\text{Al3O}_4]$ tetrahedra and $[\text{AlO}_6]$ octahedra, which connect each other by corner-sharing and edge-sharing to form a three-dimensional structure (Fig. 1a). This rigid structure feature could reduce the structural relaxation of the luminescence center in the excited state and prefer a narrow-band emission.^{28,29} Furthermore, it could also be of benefit to obtain a phosphor with low thermal quenching. It is worth noting that the $[\text{Mg}/\text{AlO}_4]$ tetrahedra are isolated and they can't connect each other. Viewing along the c axis direction (Fig. 1b), there are two distances between Mg1/Al3 atoms, the short distance $d = 9.7876$ Å and the long distance $d = 12.1774$ Å. These distances far outweigh the usual distances between Mg atoms observed in other known Mg-containing phosphors,^{7,17} contributing to reducing the energy transfer between activator ions doped at the Mg1 site and boosting the highly efficient narrow-band emission.²⁵ Meanwhile, the nearest distance between isolated Mg1/Al3 atoms is $d = 3.4426$ Å (Fig. 1b). There is a six-membered ring connected by corner-sharing of six $[\text{AlO}_6]$ tetrahedra between the nearest $[\text{Mg}/\text{AlO}_4]$ tetrahedra (Fig. 1c), which contributes to reducing the interactions between the activator ions doped at the nearest Mg1 site and induces a positive effect on the narrow-band emission. Considering the valence state and effective ionic radius with different coordination number (cn) (Al^{3+} : cn = 4, $r = 0.39$ Å, cn = 6, $r = 0.535$ Å; La^{3+} : cn = 12, $r = 1.36$ Å; Mg^{2+} : cn = 4, $r = 0.57$ Å; Mn^{2+} : cn = 4, $r = 0.66$ Å, cn = 6, $r = 0.67$ Å) and green emission of LMAO:0.28 Mn^{2+} (Fig. 1e(iii), Fig. 2a),³⁰ it is rational that Mn^{2+} tends to occupy the Mg^{2+} site. The as-synthesized sample LMAO:0.28 Mn^{2+} was investigated on XRD Rietveld refinement by Topas 5.³¹ The observed and calculated X-ray powder diffraction patterns for LMAO:0.28 Mn^{2+} , as well as the difference profile of the Rietveld refinement are illustrated in Fig. 1d. The results of Rietveld refinement for LMAO:0.28 Mn^{2+} are summarized in Table S1 (ESI[†]). All refined crystallographic parameters well satisfy the conditions, and good fits are obtained with $R_p = 3.86$, $R_{wp} = 5.16$ and $\text{GOF} = 1.60$. The refined crystallographic parameters are slightly bigger than the host,²⁷ indicating the substitution of Mg^{2+} by Mn^{2+} . Furthermore, the LMAO:0.28 Mn^{2+} microcrystal sample exhibits a spindle shape in the optical microscopy (Fig. 1e(i)), which shows a bright shine under the polarized lens (Fig. 1e(ii)), indicating the good crystallization. Under 365 nm excitation, the LMAO:0.28 Mn^{2+} sample shows bright green light in the dark environment (Fig. 1e(iii)). The spindle shape of LMAO:0.28 Mn^{2+} particles is also seen in the SEM image with a size ~ 50 μm (Fig. 1e(iv)). The SEM-EDS element mapping results demonstrate that the as-prepared sample contains La, Mg, Al, O and Mn elements (Fig. 1e(v–ix)), which are homogeneously distributed in the phosphor particles. Moreover, the uniform Mn element distribution further supports that Mn^{2+} penetrates the LMAO structure and the substitution of Mg^{2+} . The typical selected-area electron diffraction (SAED) image and the high resolution TEM (HRTEM) image taken from a fragment of the spindle sample demonstrate that the as-prepared LMAO:0.28 Mn^{2+} is a single crystal, as shown in Fig. S2 (ESI[†]).

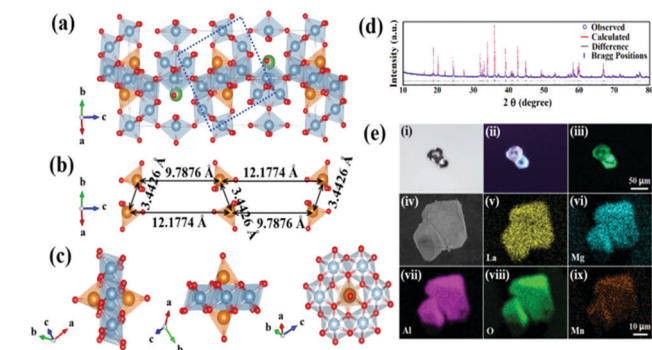


Fig. 1 (a) The crystal structure of LMAO. La atoms (green); Mg atoms (brown); Al atoms (light gray); O atoms (red). (b) The isolated $[\text{MgO}_4]$ tetrahedra in the crystal structure. (c) The connection of the nearest isolated $[\text{Mg1}/\text{Al3O}_4]$ tetrahedra by a six-membered ring from different directions. (d) The Rietveld refinement XRD pattern of LMAO:0.28 Mn^{2+} . (e) i–iii: Optical microscopy images of LMAO:0.28 Mn^{2+} in bright field (i), under the polarized lens in bright field (ii) and excited by a 365 nm UV lamp in dark field (iii), respectively; iv–ix: SEM image and SEM-EDS element mapping images of LMAO:0.28 Mn^{2+} .

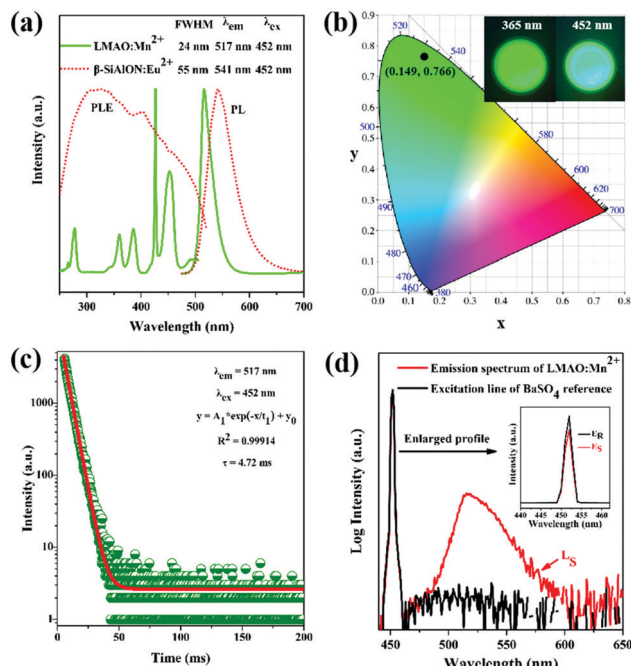


Fig. 2 (a) PLE and PL spectra of LMAO:0.28Mn²⁺ powder (green solid line) and the commercial green emitting phosphor β -SiAlON:Eu²⁺ (red dotted line), respectively. (b) The CIE chromaticity coordinate diagram for LMAO:0.28Mn²⁺ (inset figure: a digital photograph of the LMAO:0.28Mn²⁺ sample under excitation at 365 nm and 452 nm). (c) The decay curve of LMAO:0.28Mn²⁺ under excitation at 452 nm, monitored at 517 nm. (d) Excitation line of BaSO₄ and the emission spectrum of the LMAO:0.28Mn²⁺ phosphor collected by using an integrating sphere, the inset shows the magnification for the excitation line of BaSO₄ and the emission spectrum of the LMAO:0.28Mn²⁺.

The optimal Mn²⁺ content is $x = 0.28$ for LMAO: x Mn²⁺ ($x = 0.04$ – 0.68) (Fig. S3, ESI[†]), which is a considerably higher value than that of usual phosphors. Thanks to the substitution of Mg²⁺ by Mn²⁺ at the Mg1 site, LMAO:0.28Mn²⁺ exhibits an exciting ultra-narrow-band green emission peaking at 517 nm with a FWHM of ~ 24 nm under 452 nm excitation (Fig. 2a). The as-prepared LMAO:0.28Mn²⁺ sample shows an intense green light under 365 nm and 452 nm lamp irradiation (Fig. 2b inset picture). The photoluminescence excitation (PLE) spectrum of LMAO:0.28Mn²⁺ monitored at 517 nm exhibits a broad band from 275 to 500 nm, indicating that it can be excited by UV and blue light. Compared with the LMAO host, LMAO:0.28Mn²⁺ shows a characteristic absorption of Mn²⁺ in the range of 250–500 nm (Fig. S4, ESI[†]), corresponding to its PLE (Fig. 2a). Surprisingly, the self-reduction phenomenon of Mn is discovered and the emission intensities are equal for LMAO:0.28Mn²⁺ synthesized in air conditions and a 10%H₂/90%N₂ atmosphere (Fig. S5, ESI[†]), indicating that it has an extremely low preparation cost and a very great commercial potential. The commercial β -SiAlON:Eu²⁺ is chosen as a reference to compare the optical performance. β -SiAlON:Eu²⁺ shows a narrow-band emission peaking at 541 nm with a FWHM ~ 55 nm under 452 nm excitation (Fig. 2a). LMAO:0.28Mn²⁺ shows a much narrower emission band than β -SiAlON:Eu²⁺,

indicating that LMAO:Mn²⁺ is more suitable for wide color-gamut display backlights. The Commission Internationale de l'Eclairage (CIE) chromaticity coordinates of LMAO:0.28Mn²⁺ are determined to be (0.149, 0.766) (Fig. 2b). The color purity of LMAO:0.28Mn²⁺ is calculated to be 83.0%, which is much higher than that of β -SiAlON:Eu²⁺ and even Sr₂MgAl₁₂O₃₆:Mn²⁺,¹⁷ indicating that LMAO:0.28Mn²⁺ can help to achieve a larger color gamut for wLED backlights. The lifetime of LMAO:0.28Mn²⁺ is calculated to be 4.72 ms (Fig. 2c), which is less than 5 ms and could avoid the smear signal in LCD displays. Furthermore, under 452 nm excitation, LMAO:0.28Mn²⁺ shows a high IQE up to 97.6% at room temperature (Fig. 2d), and the calculated absorption efficiency (AE) and external quantum efficiency (EQE) are 26.4% and 25.8%, respectively. Under 426 nm excitation, the IQE of the LMAO:0.28Mn²⁺ phosphor is up to 99.6%, and the calculated AE and EQE are 16.1% and 16.0%, respectively (Fig. S6, ESI[†]).

Thermal stability is a key factor for phosphors in practical wLED applications. The temperature-dependent PL properties of LMAO:0.28Mn²⁺ are investigated under 452 nm excitation in the temperature range of 298–473 K (Fig. 3a and b). The relative peak intensity of LMAO:0.28Mn²⁺ drops from the original 100% at 298 K to 92.3% at 423 K (Fig. 3c), while the integrated intensity does not show any decrease when the temperature increases from 298 K to 473 K and can increase to 110.1% at 423 K, which can be ascribed to the temperature-induced emission band broadening (FWHM increasing from 24 to 33 nm, Fig. 3c). The results indicate that LMAO:0.28Mn²⁺ exhibits an excellent thermal quenching resistance property, which even is better than that of β -SiAlON:Eu²⁺ (Fig. S7, ESI[†]).³² Interestingly, the emission peak position of the LMAO:0.28Mn²⁺ phosphor barely shifts (Fig. 3b). As the temperature increases, the color coordinates of LMAO:0.28Mn²⁺ show a tiny

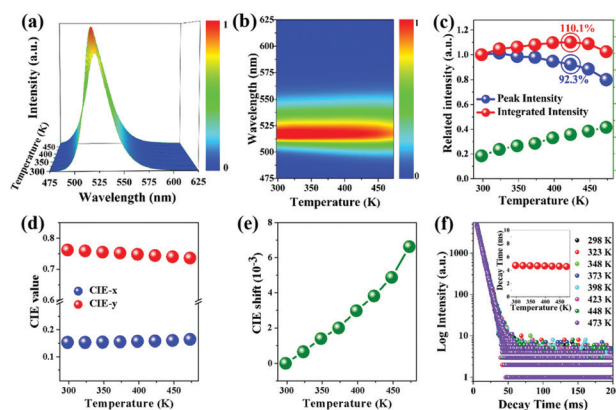


Fig. 3 (a) Temperature-dependent emission spectra of LMAO:0.28Mn²⁺ recorded at temperatures from 298 to 473 K. (b) The temperature-dependent emission intensities of LMAO:0.28Mn²⁺ in the wavelength range of 475–625 nm. (c) Normalized integrated intensities, peak intensities, and the variation of the FWHM of LMAO:0.28Mn²⁺ depending on increasing temperature. (d) Chromaticity coordinate values and (e) chromaticity shift of LMAO:0.28Mn²⁺ at different temperatures. (f) The decay curves and the decay times (inset figure) of LMAO:0.28Mn²⁺ at various temperatures.

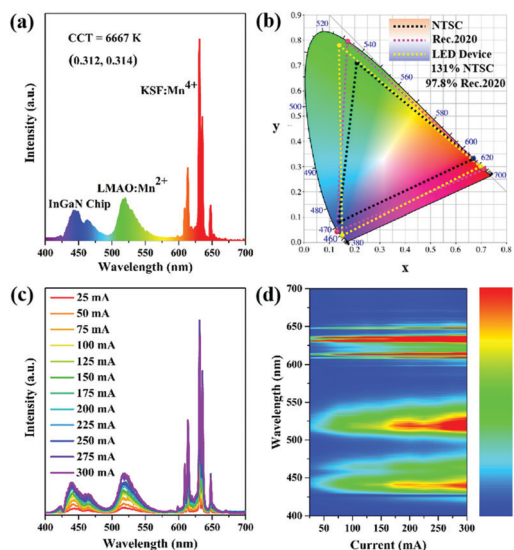


Fig. 4 (a) Electroluminescence spectrum of the wLED fabricated by the as-prepared LMAO:0.28Mn²⁺, KSF:Mn⁴⁺, and 450 nm blue chip under a current of 20 mA. (b) Color gamut of the NTSC value, and Rec. 2020 value for the fabricated LED device in the 1931 CIE system. (c) Electroluminescence spectra and (d) current-dependent emission intensities of the fabricated LED device in the current range of 25–300 mA.

variation (Fig. 3d). Correspondingly, the chromaticity shifts of LMAO:0.28Mn²⁺ exhibit a surprisingly and extremely tiny change, 3.82‰ at 423 K and 6.63‰ at 473 K (Fig. 3e), which are much better than that of other reported phosphors.^{33–36} The results indicate that the LMAO:0.28Mn²⁺ phosphor exhibits an excellent resistance to temperature-dependent color drifting. The luminescence lifetimes of the phosphors usually shorten when temperature-dependent quenching occurs due to an additional nonradiative contribution to the decay process.²⁶ Interestingly, the lifetime of LMAO:0.28Mn²⁺ barely changes from 4.72 to 4.55 ms with the temperature increasing from 298 K to 473 K (Fig. 3f), confirming the excellent temperature-dependent PL properties of LMAO:0.28Mn²⁺.⁷

The ultra-narrow-band green emission and excellent temperature-dependent PL properties make LMAO:0.28Mn²⁺ a desirable candidate for wide color gamut backlight displays. To demonstrate the potential application in backlight displays, a white LED device is fabricated by combining the green phosphor LMAO:0.28Mn²⁺, the commercial red phosphor KSF:Mn⁴⁺ and a blue GaInP chip ($\lambda_{\text{em}} = 450$ nm). At a driven current of 20 mA, the LED device produced white light emission with a correlated color temperature (CCT) of 6667 K and the CIE chromaticity coordinates of (0.312, 0.314) (Fig. 4a). Furthermore, conventional commercial RGB color filters were used to filter the white light. After passing through the color filters, the color coordinates of RGB are (0.6979, 0.3020), (0.1385, 0.7782), and (0.1502, 0.0284), respectively, which exhibits a wide color gamut of 131% NTSC and 97.8% Rec. 2020 in CIE 1931 (Fig. 4b), which is higher than other previous reported pc-wLEDs and even some QLEDs (Table S2, ESI†). Benefiting from the excellent temperature-dependent PL properties of

LMAO:0.28Mn²⁺, the luminescence intensity of the fabricated wLED device continuously increases when the driving current increases from 25 to 300 mA (Fig. 4c and d), indicating that LMAO:0.28Mn²⁺ can be applied in high power pc-wLEDs. The results indicate that LMAO:Mn²⁺ is a promising next-generation narrow-band green phosphor for wide color-gamut backlight displays.

3. Conclusions

In summary, we put forward a new strategy by doping an activator at remote isolated sites with high content to develop a high-performance ultra-narrow-band green emitting phosphor LMAO:0.28Mn²⁺. LMAO:0.28Mn²⁺ is successfully synthesized by an easily operated solid-state reaction method, which exhibits an inspiring ultra-narrow-band green emission peaking at 517 nm with a FWHM ~ 24 nm under excitation at 452 nm and a high IQE up to 97.6%. The intriguing highly efficient narrow-band emission is related with the high content Mn²⁺ occupying independently remote isolated Mg²⁺ sites. As for the LMAO:0.28Mn²⁺ phosphor, the CIE coordinates are (0.149, 0.766), and the color purity is 83.0%, and the fluorescence lifetime is 4.72 ms. More importantly, the as-prepared LMAO:0.28Mn²⁺ phosphor exhibits an outstanding thermal quenching resistance property (remaining 92.3% peak intensity and 110.1% integrated intensity at 423 K compared to the corresponding intensity at 298 K) and an excellent resistance to color drifting with chromaticity shifts of 3.82‰ at 423 K and 6.63‰ at 473 K. Exhilaratingly, the emission intensity is equal for LMAO:0.28Mn²⁺ synthesized in air conditions and in a 10%H₂/90%N₂ atmosphere, indicating that LMAO:0.28Mn²⁺ has extremely low preparation cost and very great commercial potential. By combining ultra-narrow-band green emitting LMAO:0.28Mn²⁺ and narrow-band red emitting KSF:Mn⁴⁺ with blue InGaP chips, a wLED device is fabricated with a wide color gamut of 131% NTSC and 97.8% Rec. 2020 in CIE 1931. The luminescence intensity continuously increases for the fabricated wLED device when the driving current increases from 25 to 300 mA, making LMAO:0.28Mn²⁺ a promising candidate for wide color-gamut and high-power pc-wLED backlight applications. In this work, it is inspiring to develop high-performance narrow-band green emitting phosphors by a new design strategy and accelerate the speed of discovering many new materials for wide color-gamut backlight displays.

Conflicts of interest

There are no conflicts to declare.

Acknowledgements

This work was financially supported by the National Natural Science Foundation of China (Grant No. 52002114 and 12174086).

References

- 1 M. Zhao, Q. Y. Zhang and Z. G. Xia, Narrow-band emitters in LED backlights for liquid-crystal displays, *Mater. Today*, 2020, **40**, 246.
- 2 H. Liao, M. Zhao, M. S. Molokeev, Q. Liu and Z. Xia, Learning from a mineral structure toward an ultra-narrow-band blue-emitting silicate phosphor $\text{RbNa}_3(\text{Li}_3\text{SiO}_4)_4\text{:Eu}^{2+}$, *Angew. Chem., Int. Ed.*, 2018, **57**, 11728–11731.
- 3 E. F. Schubert and J. K. Kim, Solid-state light sources getting smart, *Science*, 2005, **308**, 1274–1278.
- 4 M. Zhao, H. Liao, L. Ning, Q. Zhang, Q. Liu and Z. Xia, Next-generation narrow-band green-emitting $\text{RbLi}(\text{Li}_3\text{SiO}_4)_2\text{:Eu}^{2+}$ phosphor for backlight display application, *Adv. Mater.*, 2018, **30**, 1802489.
- 5 X. Zhang, H. C. Wang, A. C. Tang, S. Y. Lin, H. C. Tong, C. Y. Chen, Y. C. Lee, T. L. Tsai and R. S. Liu, Robust and stable narrow-band green emitter: an option for advanced wide-color-gamut backlight display, *Chem. Mater.*, 2016, **28**, 8493–8497.
- 6 B. Su, M. S. Molokeev and Z. Xia, Mn^{2+} -based narrow-band green-emitting Cs_3MnBr_5 phosphor and the performance optimization by Zn^{2+} alloying, *J. Mater. Chem. C*, 2019, **7**, 11220–11226.
- 7 E. H. Song, Y. Y. Zhou, Y. Wei, X. X. Han, Z. R. Tao, R. L. Qiu, Z. G. Xia and Q. Y. Zhang, A thermally stable narrow-band green-emitting phosphor $\text{MgAl}_2\text{O}_4\text{:Mn}^{2+}$ for wide color gamut backlight display application, *J. Mater. Chem. C*, 2019, **7**, 8192–8198.
- 8 S. X. Li, L. Wang, D. M. Tang, Y. Cho, X. J. Liu, X. T. Zhou, L. Lu, L. Zhang, T. Takeda, N. Hirosaki and R. J. Xie, Achieving high quantum efficiency narrow-band β -sialon: Eu^{2+} phosphors for high-brightness LCD backlights by reducing the Eu^{3+} luminescence killer, *Chem. Mater.*, 2018, **30**, 494–505.
- 9 R. J. Xie, N. Hirosaki, X. J. Liu, T. Takeda and H. L. Li, Crystal structure and photoluminescence of $\text{Mn}^{2+}\text{-Mg}^{2+}$ codoped gamma aluminum oxynitride (γ -ALON): A promising green phosphor for white light-emitting diodes, *Appl. Phys. Lett.*, 2008, **92**, 201905.
- 10 P. Strobel, S. Schmiechen, M. Siegert, A. Tücks, P. J. Schmidt and W. Schnick, Narrow-band green emitting nitridolithoaluminate $\text{Ba}[\text{Li}_2(\text{Al}_2\text{Si}_2)\text{N}_6]\text{:Eu}^{2+}$ with framework topology whj for LED/LCD-backlighting applications, *Chem. Mater.*, 2015, **27**, 6109–6115.
- 11 T. Takeda, N. Hirosaki, S. Funahshi and R. J. Xie, Narrow-band green-emitting phosphor $\text{Ba}_2\text{LiSi}_2\text{AlN}_{12}\text{:Eu}^{2+}$ with high thermal stability discovered by a single particle diagnosis approach, *Chem. Mater.*, 2015, **27**, 5892–5898.
- 12 Y. Ito, T. Hori, T. Kusunoki, H. Nomura and H. Kondo, A phosphor sheet and a backlight system providing wider color gamut for LCDs, *J. Soc. Inf. Disp.*, 2014, **22**, 419.
- 13 H. X. Liao, M. Zhao, Y. Y. Zhou, M. S. Molokeev, Q. L. Liu, Q. Y. Zhang and Z. G. Xia, Polyhedron transformation toward stable narrow-band green phosphors for wide-color-gamut liquid crystal display, *Adv. Funct. Mater.*, 2019, **29**, 1901988.
- 14 C. Bertail, S. Maron, V. Buissette, T. L. Mercier, T. Gacoin and J. P. Boilot, Structural and photoluminescent properties of $\text{Zn}_2\text{SiO}_4\text{:Mn}^{2+}$ nanoparticles prepared by a protected annealing process, *Chem. Mater.*, 2011, **23**, 2961.
- 15 H. R. Li, Y. J. Liang, S. Q. Liu, W. L. Zhang, Y. Y. Bi, Y. M. Gong and W. Lei, Highly efficient green-emitting phosphor $\text{BaZnAl}_{10}\text{O}_{17}\text{:Mn}^{2+}$ with ultra-narrow band and extremely low thermal quenching for wide color gamut LCD backlights, *Adv. Opt. Mater.*, 2021, **9**, 2100799.
- 16 J. Zhou, Y. H. Wang, B. T. Liu and Y. H. Lu, Effect of H_3BO_3 on structure and photoluminescence of $\text{BaAl}_{12}\text{O}_{19}\text{:Mn}^{2+}$ phosphor under VUV excitation, *J. Alloys Compd.*, 2009, **484**, 439.
- 17 Y. L. Zhu, Y. J. Liang, S. Q. Liu, H. R. Li and J. H. Chen, Narrow-band green-emitting $\text{Sr}_2\text{MgAl}_{22}\text{O}_{36}\text{:Mn}^{2+}$ phosphors with superior thermal stability and wide color gamut for backlighting display applications, *Adv. Opt. Mater.*, 2019, **7**, 1801419.
- 18 Q. Zhou, L. Dolgov, A. M. Srivastava, L. Zhou, Z. L. Wang, J. X. Shi, M. D. Drami Anin, M. G. Brik and M. M. Wu, Mn^{2+} and Mn^{4+} red phosphors: synthesis, luminescence and applications in WLEDs. A review, *J. Mater. Chem. C*, 2018, **6**, 2652.
- 19 L. Wu, S. J. Sun, Y. X. Bai, Z. G. Xia, L. W. Wu, H. M. Chen, L. R. Zheng, H. Yi, T. Q. Sun, Y. F. Kong, Y. Zhang and J. J. Xu, Defect-induced self-reduction and anti-thermal quenching in $\text{NaZn}(\text{PO}_3)_3\text{:Mn}^{2+}$ red phosphor, *Adv. Opt. Mater.*, 2021, **9**, 2100870.
- 20 G. Blasse, Luminescence of inorganic solids: from isolated centres to concentrated systems, *Prog. Solid State Chem.*, 1988, **18**, 79–171.
- 21 L. Amidani, K. Korthout, J. J. Joos, M. van der Linden, H. F. Sijbom, A. Meijerink, D. Poelman, P. F. Smet and P. Glatzel, Oxidation and luminescence quenching of europium in $\text{BaMgAl}_{10}\text{O}_{17}$ blue phosphors, *Chem. Mater.*, 2017, **29**, 10122–10129.
- 22 T. Senden, R. J.-A. van Dijk-Moes and A. Meijerink, Quenching of the red Mn^{4+} luminescence in Mn^{4+} -doped fluoride LED phosphors, *Light: Sci. Appl.*, 2018, **7**, 1–13.
- 23 D. L. Dexter and J. H. Schulman, Theory of concentration quenching in inorganic phosphors, *J. Chem. Phys.*, 1954, **22**, 1063.
- 24 H. M. Chen, L. W. Wu, F. Bo, J. K. Jian, L. Wu, H. W. Zhang, L. R. Zheng, Y. F. Kong, Y. Zhang and J. J. Xu, Coexistence of self-reduction from Mn^{4+} to Mn^{2+} and elasto-mechano-luminescence in diphase $\text{KZn}(\text{PO}_3)_3\text{:Mn}^{2+}$, *J. Mater. Chem. C*, 2019, **7**, 7096–7103.
- 25 G. J. Zhou, Z. Y. Liu, J. L. Huang, M. S. Molokeev, Z. W. Xiao, C. G. Ma and Z. G. Xia, Unraveling the near-unity narrow-band green emission in zero-dimensional Mn^{2+} -based metal halides: A case study of $(\text{C}_{10}\text{H}_6\text{N})_2\text{Zn}_{1-x}\text{Mn}_x\text{Br}_4$ solid solutions, *J. Phys. Chem. Lett.*, 2020, **11**, 5956–5962.
- 26 C. Li, X. M. Wang, F. F. Chi, Z. P. Yang and H. Jiao, A narrow-band blue emitting phosphor $\text{Ca}_8\text{Mg}_7\text{Si}_9\text{N}_{22}\text{:Eu}^{2+}$ for pc-LEDs, *J. Mater. Chem. C*, 2019, **7**, 3730–3734.
- 27 R. Brandt and B. Müller, Ein Beitrag zur kristallchemie der lanthanoidmagnetoplumbite, *Z. Anorg. Allg. Chem.*, 1984, **510**, 163–168.

- 28 P. Pust, V. Weiler, C. Hecht, A. Tucks, A. S. Wochnik, A. K. Henss, D. Wiechert, C. Scheu, P. J. Schmidt and W. Schnick, Narrow-band red-emitting $\text{Sr}[\text{LiAl}_3\text{N}_4]:\text{Eu}^{2+}$ as a next-generation LED-phosphor material, *Nat. Mater.*, 2014, **13**, 891–896.
- 29 J. L. Leñaño Jr., M. H. Fang and R. S. Liu, Critical review-narrow-band emission of nitride phosphors for light-emitting diodes: perspectives and opportunities, *ECS J. Solid State Sci. Technol.*, 2017, **7**, R3111.
- 30 R. D. Shannon, Revised effective ionic radii and systematic studies of interatomic distances in halides and chalcogenides, *Acta Crystallogr., Sect. A: Cryst. Phys., Diff., Theor. Gen. Crystallogr.*, 1976, **32**, 751–767.
- 31 A. Coelho, *Topas-A: General profile and structure analysis software for powder diffraction data*, Bruker-AXS: Madison, WI, 2005.
- 32 R. J. Xie, N. Hirotsaki, H. L. Li, Y. Q. Li and M. Mitomo, Synthesis and photoluminescence properties of β -sialon: Eu^{2+} ($\text{Si}_{6-z}\text{Al}_z\text{O}_z\text{N}_{8-z}:\text{Eu}^{2+}$): A promising green oxynitride phosphor for white light-emitting diodes, *J. Electrochem. Soc.*, 2007, **154**, J314.
- 33 J. Wang, C. C. Tsai, W. C. Cheng, M. H. Chen, C. H. Chung and W. H. Cheng, High thermal stability of phosphor-converted white light-emitting diodes employing Ce:YAG-doped glass, *IEEE J. Sel. Top. Quantum Electron.*, 2011, **17**, 741–746.
- 34 X. J. Zhang, L. Huang, F. J. Pan, M. M. Wu, J. Wang, Y. Chen and Q. Su, Highly thermally stable single-component white-emitting silicate glass for organic-resin-free white-light-emitting diodes, *ACS Appl. Mater. Interfaces*, 2014, **6**, 2709–2717.
- 35 C. Li, H. Zheng, H. Wei, S. Qiu, L. Xu, X. Wang and H. Jiao, A color tunable and white light emitting $\text{Ca}_2\text{Si}_5\text{N}_8:\text{Ce}^{3+}, \text{Eu}^{2+}$ phosphor via efficient energy transfer for near-UV white LEDs, *Dalton Trans.*, 2018, **47**, 6860–6867.
- 36 C. Li, X. M. Wang, Z. P. Yang and H. Jiao, $\text{Ca}_8\text{Mg}_7\text{Si}_9\text{N}_{22}:\text{Ce}^{3+}$ -a yellow-emitting nitride phosphor for white light emitting diodes, *ACS Appl. Electron. Mater.*, 2020, **2**, 936.